Supporting Information

Lu *et al.* 10.1073/pnas.0710800105

SI Text

Inhibition of βPGM by α-Galactose 1-Phosphate. Whereas the βPGM aspartylphosphate catalyzes the phosphorylation of the C (6)OH of α-galactose-1-phosphate, it does not catalyze the phosphorylation of the Asp using the C (1)phosphate of the α-galactose 1-phosphate or α-galactose 1,6-bisphosphate as the phosphoryl donor. Thus, α-galactose 1-phosphate is an ideal ligand to use in the study of the structure of the enzyme-substrate complex.

Small Molecule Data for Mononuclear Pentacoordinate Tungstate. A search of the Cambridge Small-Molecule Database for available structures of tungstate with five ligands to oxygen reveals that the majority of such structures are highly constrained ring structures possessing four oxygen ligands in a plane and the fifth in an apical position {with geometry similar to octahedral minus one apical ligand [e.g., accession code JAFWAO (1)]}. The structures that maintain perfect or distorted trigonal bipyramidal pentacoordinate geometry have at least one nonoxygen atom, such as Cl [accession code ILOHAS (2)] or carbon [accession code DAVMOC (3)].

Enzyme Complexes with Pentacoordinate Tungstate. These enzymes were cocrystallized with tungstate and adenosine to form a coordination complex within the respective active sites that depicts the expected intermediate/transition state formed along the reaction coordinate. The His side chain occupies an apical position (His NE2, 2.5Å) and the adenosine ligand assumes an equatorial position (1.72Å). Because the adenosine is not the leaving group, and only the leaving group occupies an apical position in the transition states of phosphoryl transfer reactions (4), this structure represents the first snap shot of an enzyme that distorts the coordination geometry of tungstate to conform to the steric/electrostatic environment of the catalytic site that by design complements the transition state.

Bond Lengths for Mononuclear Vanadate. The distance between the Asp-8 carboxylate oxygen atom and the vanadium atom (2.0 ± 0.09 Å) is consistent with a covalent bond as is the distance to the other three oxygen atoms (1.7–1.8 ± 0.09 Å). These values fall within the calculated bond lengths for tetracoordinate vanadate dimethyl esters (1.62–1.64 Å for non-bridging and 1.82–1.84 Å for bridging) and experimentally observed bridging V–O bonds in pentacoordinate and hexacoordinate species of 1.85 Å and 1.8–2.0 Å, respectively (5).

Assignment of D10A/vanadate Structure. Examination of the difference electron density maps for HPP-D10A/vanadate calculated with the coefficients $F_o - F_c$ shows that there is no density in the position occupied by the apical oxygen of the pentavalent vanadate structure. Thus, the observed electron density does not represent an average of that of a low occupancy pentacoordinate vanadate and orthovanadate (estimated upper limit <10%). It is consistent with a distorted tetrahedral vanadate with a single ligand to the nucleophilic Asp-8.

Supplementary Materials and Methods

Materials

Except where indicated, all chemicals were obtained from Sigma–Aldrich. The Biolmol green phosphate assay kit was purchased from Biolmol Research Laboratories. Primers, T4 DNA ligase, and restriction enzymes were from Invitrogen. *Pfu*, *pfu* Turbo polymerases and the pET3 vector kit were from Stratagene. The Geneclean Spin Kit and the Qiaprep Spin Miniprep Kit were from Qiagen. Host cells were purchased from Novagen.

Site-Directed Mutagenesis, Expression, and Purification. The cloning and purification of native HPP was reported in ref. 6. The Quick change method (7) was used to generate D10A mutant, using mutagenesis primer (5′-TTTGATATAGCCGGAACG, and 5′-CGTTCCGGCTATATCAAA). The sequences of plasmid DNA were confirmed by sequencing carried out by the Tufts University Core Facility. The D10A mutant of HPP was purified in the same manner as that was used to purify wild-type HPP (6).

Steady-State Kinetics. The purified proteins were concentrated with a Centricon-10 (Millipore) and dialyzed against buffer A [50 mM Hepes (pH 7.0)] before using in kinetic studies. The steady-state kinetic parameters (K_m and k_{cat}) of phosphorylated substrates *p*-nitrophenyl phosphate (*PNPP*) and β-D-glucose 6-phosphate were determined from initial reaction velocities measured at varying substrate concentrations (ranging from 0.5–5 K_m), and the resulting data were fitted to the Michaelis–Menten equations as described in ref. 6.

Activity Assays. The rate of *p*-nitrophenyl phosphate (PNPP) hydrolysis was determined by monitoring the increase in absorbance at 410 nm ($\Delta\varepsilon = 18.4\ mM^{-1}\cdot cm^{-1}$) (8) at 37°C. The 0.5-ml assay mixtures contained 50 mM Hepes (pH 7.0), 5 mM $MgCl_2$, and various concentrations of PNPP.

The rate of β-D-glucose 6-phosphate hydrolysis was determined by monitoring the rate of NADPH (340 nm; $\Delta\varepsilon = 6.22\ mM^{-1}\cdot cm^{-1}$) formation in a 0.5-ml coupled assay solution initially containing 50 mM Hepes (pH 7.0; 37°C), 5 mM $MgCl_2$, 0.2 mM $NADP^+$, and 1 unit of glucose dehydrogenase (E.C. 1.1.1.119) (Sigma–Aldrich). The kinetic constants determined with this assay agreed with those determined using the fixed time phosphate assay.

1. Bickelhaupt FM, Neumuller B, Plate M, Dehnicke K (1998) Crystal structure and bonding of [W(O-t-Bu)(4)(THF)]. *Zeitschrift Fur Anorganische Und Allgemeine Chemie* 624:1455–1459.
2. Veige AS, *et al.* (2003) Symmetry and geometry considerations of atom transfer: Deoxygenation of (silox)(3)WNO and R3PO (R = Me, Ph, Bu-t) by (silox)(3)M (M = V, NbL (L = PMe3, 4-picoline), Ta; silox = (Bu3SiO)-Bu-t). *Inorg Chem* 42:6204–6224.
3. Feinsteinjaffe I, Dewan JC, Schrock RR (1985) Preparation of anionic tungsten(Vi) alkyl complexes containing oxo or sulfido ligands and the x-ray structure of [N(C2h5)4](Wo2[Oc(Ch3)2c(Ch3)2o][Ch2c(Ch3)3]. *Organometallics* 4:1189–1193.
4. Westheimer FH (1968) Pseudo-rotation in the hydrolysis of phosphate esters. *Acc Chem Res* 1:70–78.
5. Borden J, Crans DC, Florian J (2006) Transition state analogues for nucleotidyl transfer reactions: Structure and stability of pentavalent vanadate and phosphate ester dianions. *J Phys Chem B* 110:14988–14999.
6. Lu Z, Dunaway-Mariano D, Allen KN (2005) HAD superfamily phosphotransferase substrate diversification: Structure and function analysis of HAD subclass IIB sugar phosphatase BT4131. *Biochemistry* 44:8684–96.
7. Wang W, Malcolm BA (1999) Two-stage PCR protocol allowing introduction of multiple mutations, deletions and insertions using QuikChangeTM site-directed mutagenesis. *BioTechniques* 26:680–682.
8. Shin DH, *et al.* (2003) Crystal structure of a phosphatase with a unique substrate binding domain from Thermotoga maritima. *Protein Sci* 12:1464–1472.

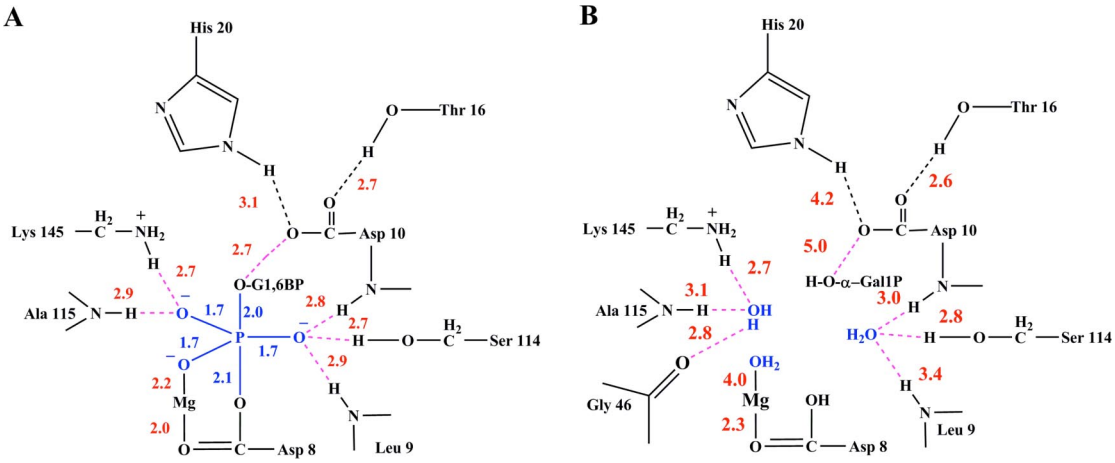

Fig. S1. Schematic of the bond lengths (in *Å*) and contributing residues in active and inhibited complexes. (*A*) The βPGM(Mg^{2+})(glucose-6-phosphate-1-aspartylphosphorane intermediate. (*B*) The inhibitor α-galactose-1-phosphate binds with three water molecules. Distances are depicted as dashed lines.

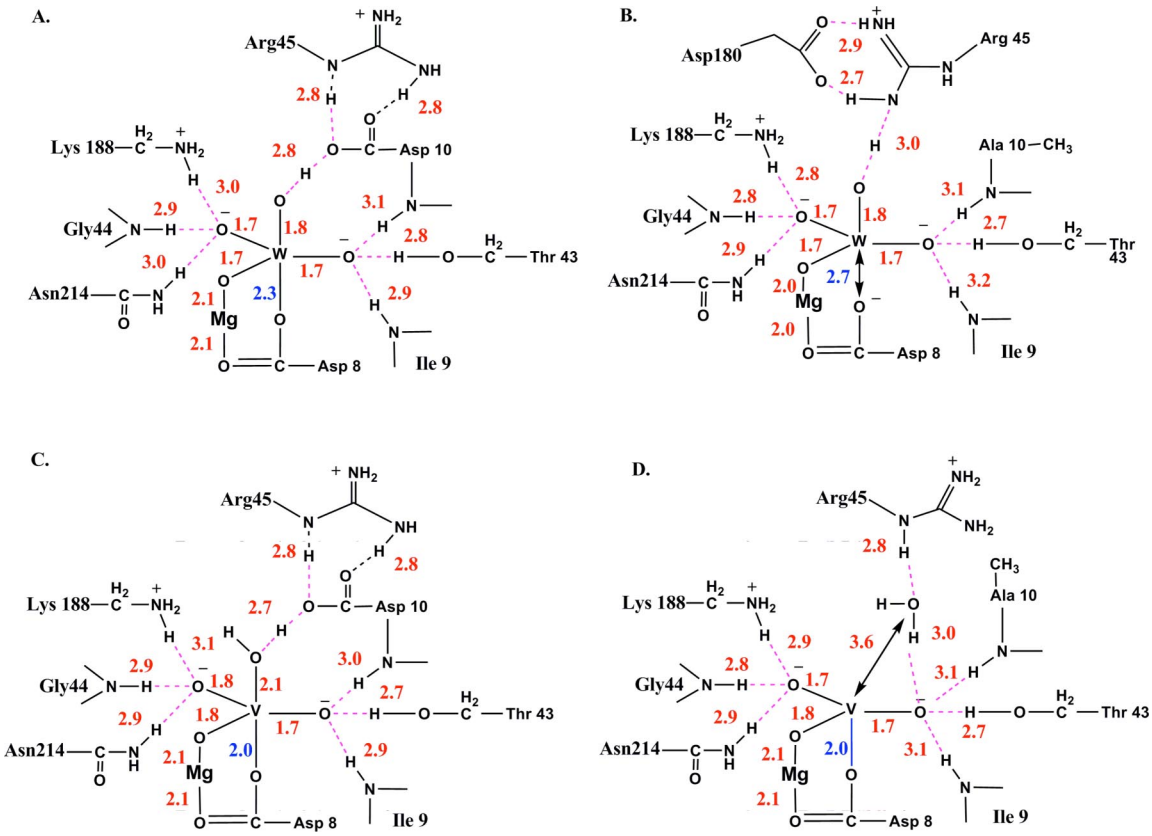

Fig. S2. Schematic of the bond lengths (in Å) and contributing residues in complexes with phosphate mimics. (*A*) The wild-type HPP-tungstate complex. (*B*) The mutant HPP-D10A-tungstate complex. (*C*) The wild-type HPP-vanadate complex. (*D*) The mutant HPP-D10A-vanadate complex. Hydrogen bonds depicted as dashed lines, and distances are shown as double-headed arrows.

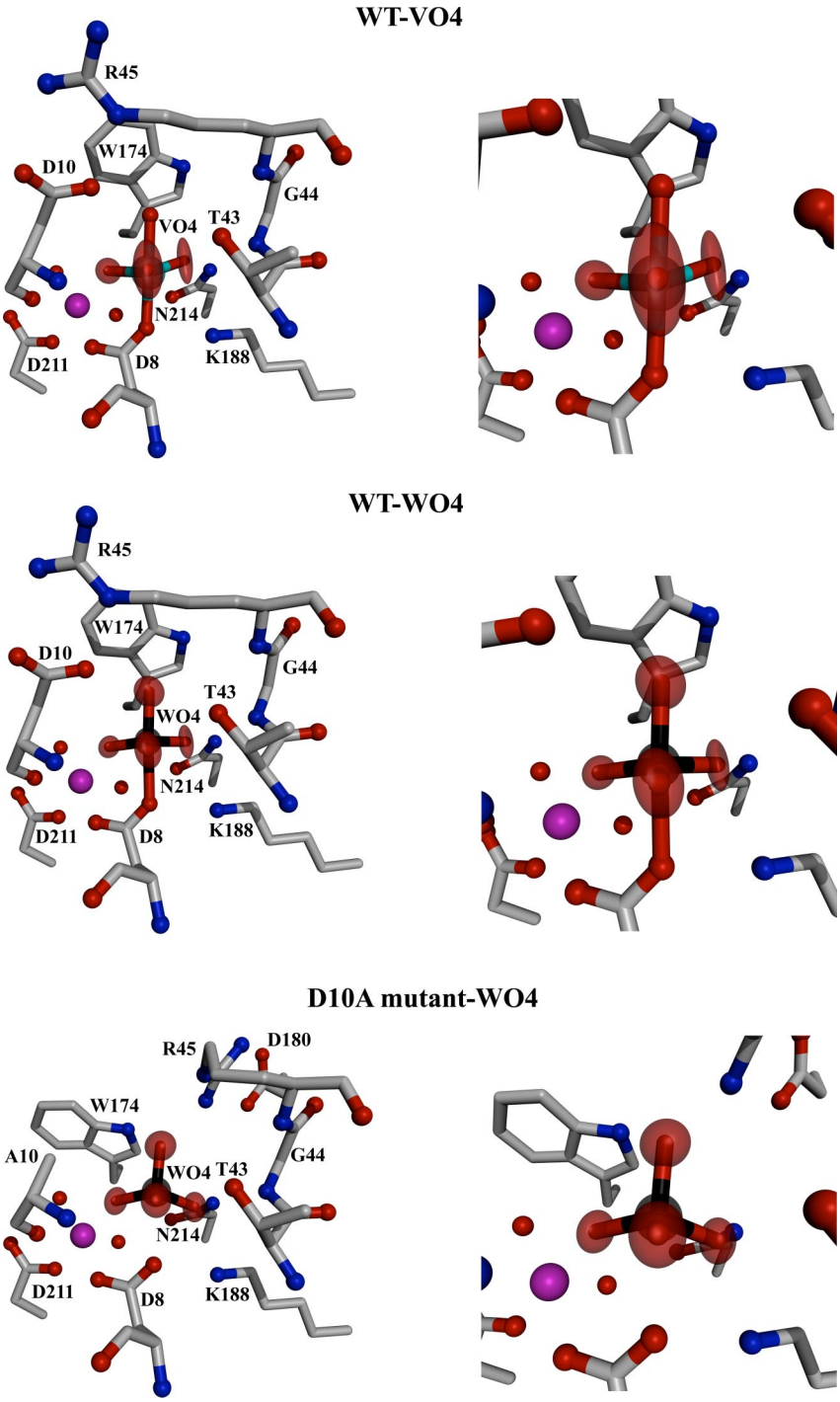

Fig. S3. Depiction of the HPP active site in the presence of phosphate mimics and the cofactor Mg^{2+} (magenta sphere). The ligands are depicted as ORTEP diagrams with the anisotropic B-factors connoted in magnitude and directionality by ellipses. Each ligand is magnified at *Right*. (*Top*) The 1.00 Å resolution structure of HPP complexed with vanadate. (*Middle*) The 1.03 Å resolution structure of HPP complexed with tungstate. (*Lower*) The 1.07 Å structure of structure of D10A HPP complexed with tungstate.

Table S1. Additional refinement statistics

Parameter	Wild-type HPP/WO_4^{2-}	Wild-type HPP/ VO_4^{3-}	HPP-D10A / WO_4^{2-}	HPP-D10A / VO_4^{3-}
No. protein/water atoms per asu	2025/501	2025/461	2022/520	2022/447
No. Mg^{2+} /No. VO_4^{3-} or WO_4^{2-} ion per asu	1/1	1/1	1/1	1/1
Average B-factor, $Å^2$	26.0	26.1	28.2	19.4
Protein	13.5	15.1	15.9	16.8
Main chain atoms	11.9	13.5	14.2	15.0
Solvent	32.5	32.5	34.4	28.8
Mg^{2+}	8.0	9.8	10.7	14.3
Ligand	9.7	14.7	11.1	13.7
Luzzati coordinate error, Å	0.12	0.15	0.12	0.16
Matrix-Inversion error length, Å; angle, deg.	0.043, 2.3	0.041, 2.5	0.064, 3.4	NA
Rmsd				
Bond length, Å	0.025	0.033	0.021	0.036
Dihedrals, deg.	24.3	24.2	24.3	24.4
Angles, deg.	2.2	2.5	2.1	2.6
Impropers, deg.	1.72	2.15	1.61	2.00